UC Berkeley
UC Berkeley Previously Published Works

Title
Vibrational and electronic dynamics of nitrogen-vacancy centres in diamond revealed by two-dimensional ultrafast spectroscopy

Permalink
https://escholarship.org/uc/item/67v876g6

Journal
Nature Physics, 9(11)

ISSN
1745-2473 1745-2481

Authors
Huxter, V M
Oliver, T AA
Budker, D
et al.

Publication Date
2013-09-29

DOI
10.1038/NPHYS2753

Peer reviewed

eScholarship.org Powered by the California Digital Library
University of California

Vibrational and Electronic Dynamics of Nitrogen-Vacancy Diamond Revealed by Two-Dimensional Ultrafast Spectroscopy

V. M. Huxter,* T. A. A. Oliver, and G. R. Fleming†

Department of Chemistry, University of California,

Berkeley and Physical Bioscience Division,

Lawrence Berkeley National Laboratory, Berkeley, CA, USA 94720

D. Budker

Department of Physics, University of California,

Berkeley and Nuclear Science Division,

Lawrence Berkeley National Laboratory, Berkeley, CA, USA 94720

The optical and material properties of negatively charged nitrogen-vacancy (NV) centers in diamond make them attractive for applications ranging from quantum information to electromagnetic sensing. These properties are strongly dependent on the vibrational manifold associated with the center, which determines phenomena associated with decoherence, relaxation and spin-orbit coupling. Despite its paramount importance in tuning these properties, the role of the vibrational bath and its effect on the electronic state dynamics of NV centers in diamond is not fully understood. To elucidate the role of the bath, we present two-dimensional electronic spectroscopic studies of ensembles of NV defect centers in diamond (NV-diamond). We observe picosecond non-radiative relaxation within the phonon sideband and find that strongly coupled local modes dominate the vibrational bath. These findings provide a starting point for new insights into dephasing, spin addressing and relaxation in NV-diamond with broad implications for magnetometry, quantum information, nanophotonics, sensing, and ultrafast spectroscopy.

Diamond can stably accommodate a variety of defects, each of which has its own characteristic properties. One particular defect, called the nitrogen-vacancy center, consists of a nitrogen substitution with a nearest-neighbor-vacancy point defect in the carbon lattice. When negatively charged, the NV center has a unique combination of spin and optical properties, accommodating remarkable spin coherences of up to one second at room temperature [1]. As a quantum solid-state system, NV centers are particularly promising due to their optically and magnetically addressable spin coherences, fast spin manipulation [2], and coupling to adjacent electronic and nuclear spins [3]. These systems have wide ranging applications including solid-state qubits [1, 3, 4], ultrasensitive magnetometers [5, 6], single-photon emitters [7], and ultra-resolution imaging [8].

In a diamond system containing negatively charged NV centers, the spin states can be initialized and read out by accessing an optical transition between triplet states due to an intersystem-crossing pathway. While the nanosecond decay of the electronic state has been investigated in earlier work [9–11], ultrafast picosecond and femtosecond dynamics associated with coherent vibrational motion and internal conversion pathways remain entirely unexamined. In addition to the electronic levels, NV-diamond systems have significant phonon sidebands. The vibrational modes in these sidebands are strongly coupled to the

NV center [12–14], influencing the decoherence of the spin state and dephasing in the excited state [9], the flow of energy through the system, and the optical transitions [15]. Understanding the dynamics of the vibrational bath is critical to understanding the optical dephasing of the system and thus to applications involving optically driven quantum effects. Beyond applications related to the quantum mechanical properties, the interaction between electronic states and vibrational modes in the NV-diamond system provides us with critical information on its fundamental properties with implications for its use in nanophotonics, sensing, magnetometry, and NMR.

In order to elucidate the relaxation pathways of this solid-state quantum system, we present the first ultrafast optical measurements on NV-diamond. Using two dimensional electronic spectroscopy (2DES) [16–18], the dynamics of both the electronic and vibrational relaxation pathways in NV-diamond are measured on femtosecond timescales. This time resolution allows us to observe coherent vibrational dynamics and relaxation through the phonon sideband in real time. 2DES allows us to create an energy-dynamic map of the system, tracing out the vibrational and electronic relaxation pathways through coherences and populations, vibrational and electronic states. 2DES is a powerful spectroscopic technique that provides a means of correlating the initial absorption interaction with the final emission. Using the 2DES experiment, we find that the spectrum of the NV center is dominated by individual local vibrational modes. By constructing a discrete spectral density using the experimentally determined frequencies we model the linear and nonlinear optical signals, demonstrating the importance of the local modes in the vibrational bath.

A simplified schematic of the NV-diamond energy level structure is shown in Fig. 1(a). The ^3A and ^3E states are split into $m_s = \pm 1$ and $m_s = 0$ spin sublevels. While the spin states are not directly observable in the electronic optical measurements, they are affected by the electronic and vibrational transitions that are the subject of the current work. Singlet states, with an energy gap corresponding to the near infrared [11, 19, 20], are not optically excited or probed in the current measurement. The absorption spectrum of the NV-diamond sample used in the experiment is shown in Fig. 1(b). The zero-phonon line (ZPL), which in a linear measurement corresponds to transitions between the ground and excited state occurring without the assistance of a vibration, is at 15700 cm^{-1} (638 nm) and persists at room temperature in NV-diamond. The broad feature to the high-energy side of the ZPL is the phonon sideband which spans more than 300 meV at room temperature. In

the linear absorption spectrum some vibronic structure, associated with vibrational states that are strongly coupled to the electronic transition, is apparent in the phonon sideband. This structure is clearly highlighted in the second derivative of the absorption spectrum shown in Fig. 1(c).

As a chromophore, the NV defect can be described as a strongly vibrationally broadened two-level system. The only electronic transition is from the ground to the triplet excited state. The broad lineshape observed in the linear absorption arises solely from the phonon sideband associated with this transition. The vibrational structure in the phonon sideband, seen in the linear absorption and emphasized in its second derivative (Fig. 1 (b) and (c)), is evident in the 2DES data shown in Fig. 1(d). The vibrational contributions to the signal appear in the 2DES experiment since it follows excitation dynamics. The 2DES signal is generated by the nonlinear interaction of three ultrafast pulses with the NV-diamond sample. At each waiting time, t_2, the data are collected as a function of the time delay between the first two interactions, t_1, which are labeled as shown in Fig. 1(e). The first pulse generates a coherence between the ground and excited state that evolves during the time t_1. The second pulse puts the system in an excited or ground state population that evolves for the duration of the time delay t_2. At each waiting time, the data are Fourier transformed with respect to t_1, producing the conjugate variable ω_1, and plotted relative to the frequency dispersed emission axis, ω_3, correlating the initial absorption event with the emission. This correlation allows us to follow the evolving system through vibrational and electronic states. The 2DES plot in Fig. 1(d) was collected for a time delay, t_2 of 5 ps. At this t_2 delay, the major directly observable coherent evolution of vibrational modes has been damped out but relaxation via vibrational pathways is still apparent. These components can be seen by taking a slice at fixed ω_3 through the 2DES plot at the energy of the ZPL transition (15700 cm^{-1}). This slice, presented in Fig. 1(f), frequency resolves the contributions to the emission at the ZPL energy, showing three peaks. The peak at $\omega_1 = 15700$ cm^{-1} is attributed to stimulated emission at the same energy as the initial absorption. The other two peaks correspond to signal contributions that absorb at energies of $\omega_1 = 16180$ cm^{-1} and 16780 cm^{-1} and emit at the energy of the ZPL. These two peaks are associated with the first and second vibronic transitions observed in the linear absorption, indicating that relaxation from the phonon sideband and emission at the ZPL transition energy involves participation of vibrational components.

The 2DES experiment correlates the initial absorptive interaction with the signal emission, creating a map of absorption and emission events. Diagonal features arise when the energy of absorption and emission are the same, off-diagonal features (cross peaks) originate when they are different. In an absolute value spectrum, the features above the diagonal can arise from an excited state absorption contribution (requiring the participation of a third electronic state) or from the action of a vibrational mode excited at different points along its wavepacket trajectory [21, 22]. The peaks below the diagonal are primarily associated with energy transfer and redistribution among the nuclear degrees of freedom. In NV-diamond, the defect centers (chromophores) are electronically isolated from each other. In this system, the off-diagonal contributions do not originate from inter-chromophore energy transfer but from vibrational contributions. In Fig. 1(d) and the corresponding slice in (f), the peaks below the diagonal along the ZPL transition energy for fixed ω_3 arise from energy moving from the phonon sideband to the lowest-energy excited state through the strongly coupled electronic-vibrational transitions.

The ability to resolve the individual vibrational contributions to the emission at the energy of the ZPL is one of the major advantages of two dimensional spectroscopy. The 2DES experiment allows us to separate out the origins of the zero-phonon emission, revealing the diagonal contribution along with cross peaks associated with the vibronic modes. Spectral resolution of the signal contributions does not necessarily mean that, in a nonlinear experiment such as 2DES, all of the signal that appears at the energy of the ZPL is strictly associated with a zero-phonon transition. Instead, the 2DES plot reports non-linear absorption and emission energies and any signal with the same emission energy gap as the ZPL will appear at that emission energy. By correlating the initial absorption and emission events we can isolate different contributions to the signal, providing significant advantages as compared to other experiments. For example, the resolution of the contributions to the ZPL transition energy along the ω_1 axis would be impossible even in a frequency resolved pump-probe experiment, which integrates over the entire ω_1 axis.

Fig. 1(d) demonstrates that the primary relaxation channel for a waiting time of t_2=5 ps is via vibronic channels to the energy associated with the ZPL. At shorter waiting times, the energy is redistributed amongst multiple strongly coupled vibrational modes that beat, modifying the frequency dependence of the observed 2DES signal. This dynamic vibrational response is shown in a series of absolute-value 2DES surfaces at different waiting

times in Fig. 2. At waiting times of less than 2 ps (Fig.2 (a) – (c)), the amplitude of the spectrum above and below the diagonal oscillates in response to the action of the vibrational modes strongly coupled to the NV defect. These amplitude oscillations define a regime of vibrational coherence in the system. After approximately 2 ps, the oscillatory motion is mostly damped leaving clear peaks associated with vibronic levels.

Many vibrational contributions appear in the 2DES data and can be seen by looking at different regions of the 2DES plot. The appearance of these modes is further complicated since they appear on top of a nanosecond decay associated with the excited state lifetime. To clearly show the oscillatory behavior observed in the 2DES surfaces, we have selected a subregion associated with the first vibronic cross peak, labeled in panels (a)–(e) of Fig. 2 using a black box. The short waiting time oscillatory behavior of this region is presented in Fig. 2 (f). The bottom part of panel (f) presents the specified region integrated over the ω_1 axis and plotted with respect to the ω_3 emission axis, while the top part plots the intensity of the total integrated region defined by the black box. Panel (f) shows that there are strong, complex oscillations associated with vibrational modes in just this small subregion of the 2DES surface. By integrating over other regions or whole axes, it is possible to obtain the vibrational spectrum of the NV-diamond system.

As shown in Fig. 2, the overall 2DES signal intensity decays on a timescale of picosecond associated with non-radiative relaxation in the phonon sideband and nanoseconds associated with the excited state lifetime. At waiting times longer than 2 ps, the 2DES signal has a square shape with a distinct band at the ZPL transition energy on the emission axis. The square shape of the signal arises from the contributions of the vibronic levels. The laser spectrum used to excite the NV-diamond sample (shown in Fig. 1(b)) is peaked at 16000 cm^{-1}, which means that the majority of the excitation is into the phonon sideband.

The timescales associated with population dynamics (diagonal components of the density matrix) were recovered from the 2DES data by integrating over the 2D surfaces at each waiting time, t_2. Plotting the 2DES integrated intensity versus waiting time produces a transient grating signal (analogous to pump-probe spectroscopy). These data were then fit to a exponential decay with a picosecond and nanosecond component, where the latter is associated with excited state relaxation. The picosecond decay associated with non-radiative relaxation or internal conversion within the phonon sideband was found to be 4.2 ± 0.9 ps based on an average of five repeat measurements. This timescale is slower than

expected given the density of the vibrational states [23]. The relative slowness of internal conversion in the NV-diamond system suggests that individual strongly coupled vibrational modes dominate the relaxation process resulting in a reduced apparent density of states. Additional details regarding recovery of the transient grating signal and the measurement of the internal conversion timescale are available in the Supplementary Information.

As Fig. 2 reveals, the vibrational dynamics in NV-diamond are complex, involving a significant number of individual and overlapping vibrational modes. In order to resolve the vibrational modes coupled to the NV defect, we isolate the region of the 2DES spectrum associated with emission at the energy of the ZPL. A significant portion of the energy absorbed by the NV center relaxes via vibrational channels to the ZPL energy, providing a sub-region of the spectrum that can be analyzed to clearly isolate the vibrational modes even at long waiting times. This includes energy absorbed into the phonon sideband which relaxes to the lowest energy excited state prior to emission. The strong vibrational coupling to the ZPL transition and the fast non-radiative rate associated with internal conversion is essential to the potential applications of the NV-diamond system, especially those that rely on near monochromatic emission or optical addressing of states, since these processes rely on relaxation to the band edge and subsequent emission or relaxation via an intersystem crossing mechanism.

The specific frequencies and dynamics of the vibrational modes associated with the emission from the ZPL are shown in Fig. 3. The black rectangle in Fig. 3(a) indicates the subregion of the plot associated with emission (along the ω_3 axis) at the ZPL energy. By integrating over the emission axis of the subregion, we obtain a single trace for each waiting time consisting of the features emitting at the ZPL energy dispersed along the axis of the initial absorptive event, ω_1. This procedure effectively isolates and projects the contributions of the signal emitting at the ZPL energy onto the ω_1 axis. As shown in Fig. 3(b), these traces for individual waiting times are stacked together to create a plot that shows the evolution of the different spectral components to the emission relative to the entire range of waiting times out to 100 ps. The signal along the waiting time axis provides information on the population dynamics. Contributions associated with coherences are recovered since the signal is dispersed along the ω_1 axis and thus includes off-diagonal parts of the spectrum. In Fig. 3(b) clear oscillations associated with low-frequency modes, most likely arising from acoustic phonons in the diamond lattice, are apparent even out to tens of

picoseconds. The shorter waiting time dynamics, shown in Fig. 3(c), reveal a rich pattern of higher-frequency coherent vibrations associated with the defect.

To resolve the vibrational components, the signal in Fig. 3(b) was Fourier transformed, producing the plot in Fig. 3(d). The Fourier transform revealed a number of distinct vibrational components at frequencies in the range of 200 to 1800 cm^{-1}. Other higher-frequency modes are likely present in the system, however, they are outside of the bandwidth of the laser pulse. A number of vibrations were also present at lower frequency, forming a structured continuum of closely spaced modes. These lower-frequency modes are associated with the acoustic modes of the diamond lattice. The higher-frequency modes are strongly coupled to the defect and have a significant influence on its optical properties.

The frequencies obtained from the average of five independent 2DES experiments are

TABLE I: Discrete Frequency Components Obtained From the 2DES Measurements and Comparison to Literature Values.

$\omega_{measured}$ $(cm^{-1})^a$	$\omega_{literature}$ (cm^{-1})	ω_{theory} (cm^{-1})
182 ± 21	–	–
259 ± 19	–	255 [15]
337 ± 31	355[13]	336 [15]
457 ± 18	490 [13]	481.5, 476, 477 [24]
558 ± 16	560^b [25]	574, 582, 577 [15]
644 ± 21	677 [13]	621, 620 [24]
736 ± 18	–	734 [26]
1028 ± 22	1040 [27]	1030 [26]
1166 ± 22	1130[13, 27]	1182 [26]
1339 ± 31	1332^c [27, 28]	Raman Mode
	or 1344 [13, 27]	
1525 ± 26	1510^d [28]	1555 [26]

[a]The error estimates are based on five independent repeat measurements.

[b]Axial Mode

[c]Raman Mode

[d]There are a number of vibrations in this region associated with nitrogen defects or Raman modes

listed in Table I along with comparisons to literature values determined theoretically and experimentally. The calculated values were obtained using different theoretical methodologies to determine the predicted frequencies of modes local to the NV center. Although this comparison is not meant to be definitive, most of the experimentally observed modes match closely with calculated local modes. The frequencies obtained by previous, mostly luminescence, experiments have also been associated with local mode dynamics. Local modes are associated with deformations in the lattice within a few unit cells of the defect. The presence of the NV defect leads to a modification of the elastic moduli similar to that experienced by the dangling bonds in semiconductor nanocrystals [29]. These local modes dominate the bath comprising a major part of the dissipative response of the system.

As is evident in Table I, there is excellent agreement between vibrational modes measured in the current experiment and those in the literature either determined theoretically or experimentally. In some cases, there are multiple closely spaced modes that could be associated with the frequencies observed in the 2DES experiment. It is possible that all of those modes are present but are not unambiguously resolvable. The previously observed experimental vibrational frequencies listed in Table I were obtained entirely from steady state experiments, whereas the values obtained from the 2DES experiments were measured as they evolved in real time. This allowed direct observation of vibrational coherences and the dynamics of vibrational relaxation pathways, impossible to retrieve from previous experimental work. Additionally, observation of vibrational modes in the 2DES experiment requires that the vibration be strongly coupled to the electronic transition, providing a direct link between the optically excited NV defect and the observed frequencies.

Based on the tentative assignment to theoretical values listed in Table I, the experimentally observed modes are a combination of ground and excited state, a and e symmetry types. The peaks at 457 cm^{-1}, 558 cm^{-1} and 1028 cm^{-1} correspond to the vibronic structure in the linear absorption. The only mode without an assignment is the lowest frequency vibration at 182 cm^{-1}. The two highest frequency modes listed, 1339 and 1525 cm^{-1} are likely associated with delocalized diamond lattice dynamics. The 1525 cm^{-1} mode is an e symmetry mode [26] or an sp^2 phase Raman emission [30]. The contribution at 1339 cm^{-1} is most likely a Raman mode from the bulk diamond matrix [28] although a local mode at 1344 cm^{-1} has been experimentally observed.

From the 2DES data, we have measured a series of vibrational modes that are strongly

coupled to the NV center. In order to understand the involvement of the individual vibrational modes in the measured spectra, we used the experimental vibrational frequencies to model the 2DES signal. We calculate the linear and third order nonlinear optical response of the NV-diamond by modeling it as a vibrationally broadened two-level system. Following a response function formalism based on the work of Cho [31] and Mukamel [32], the vibrational modes were explicitly included in the spectral density which can be written as a sum of individual contributions [33]. The spectral density of the system was constructed using a Drude-Lorentz form for the quasi-contiunua of low-frequency modes (sub 100 cm^{-1}). A form of the multimode Brownian oscillator model adapted to the case of one oscillator [34, 35] was used to include the individual frequencies obtained from the 2DES experiment. (Additional details are given in the Supplementary Information.)

Simulated 2DES and linear absorption spectra are presented in Fig. 4(a) and (b), respectively. The corresponding experimental data are shown in panels (c) and (d). The simulation closely agrees with the experimental results with some deviation at higher energy. This is because the input frequencies were cut off and an approximation of the experimental laser pulse spectrum was used. Calculations performed for shorter waiting times also reproduce the oscillating amplitudes across the 2DES spectra shown in Fig. 2. In the simple two-level electronic system model, all of the broadening and structure comes from the experimentally obtained frequencies used as inputs in the spectral density. These strongly coupled local vibrational modes that dominate the vibrational bath of the NV-diamond system are sufficient to recover both the linear and the nonlinear optical response.

The vibrational modes coupled to the NV center influence spin-orbit coupling, dephasing and relaxation and are critical for the application of NV-diamond to quantum information and memory, single-photon sources, imaging and sensing. Using 2DES measurements, we have revealed the interaction between the optically excited NV defect and the vibrational bath, showing that the response of the system is determined by strongly coupled local modes. Accessing the dominant components of the vibrational bath will allow us to tune the properties of the system, providing new avenues for research. For example, by optically pumping the NV centers we could specifically excite phonon modes based on their coupling factors, allowing the development of a NV-diamond material that can be used for quantum storage and information processing based on both phonons and spin.

ACKNOWLEDGEMENTS

The authors thank Adam Gali for initially suggesting ultrafast measurements with NV-diamond, Andrey Jarmola for preparing the NV-diamond sample, Neil Manson and Pauli Kehayias for helpful discussions. V.M.H. thanks the National Science and Engineering Research Council of Canada for a postdoctoral fellowship. D.B. was supported by NSF, IMOD, and the AFOSR/DARPA QuASAR program. The work by V.M.H., T.A.A.O. and G.R.F. was supported by NSF grant CHE-1012168.

AUTHOR CONTRIBUTIONS

V. M. H., D. B. and G. R. F. conceived the experiment. D. B. and G. R. F. supervised the project. V. M. H. determined the experimental protocol, wrote and performed the simulation, analyzed the data and wrote the manuscript. V. M. H. and T. A. A. O. collected the data. All authors discussed the results and implications and commented on the manuscript at all stages.

METHODS

2DES measurements were performed using an apparatus described in detail previously [36] and are only briefly summarized here. The output from a home-built Ti:sapphire oscillator/regenerative amplifier was used to pump a non-collinear optical parametric amplifier (NOPA), generating pulses in the visible wavelength range. The NOPA output was tuned for wavelength and bandwidth to excite the ZPL and the first two strongly coupled vibronic transitions. The spectrally tuned NOPA pulses were used for the 2DES experiment, which was performed using a diffractive optic based design, where four passively phase stabilized beams were focused into the sample using a box geometry. The signal radiated in the $k_s = -k_1 + k_2 + k_3$ phase-matching direction was mixed with a weak local oscillator reference beam, spectrally dispersed using a Princeton Instruments SP2300A spectrometer and heterodyne-detected on a PIXIS 100 camera.

The 2DES data at each waiting time, t_2, were collected as a function the time delay between the first two interactions, t_1, which are labeled as shown in Fig. 1(e). To obtain the 2DES data, the time delay t_1 was scanned using matched glass wedge pairs that allow for attosecond timestep resolution without beam deviation [37]. The interferograms generated by the mixing of the signal and the local oscillator were collected for the scanned delay t_1 and Fourier transformed to produce the frequency-domain 2D spectrum for a single delay t_2. Population dynamics were obtained by repeatedly scanning t_1 for different waiting times, t_2. All of the 2DES plots shown here are absolute-value total signals. A total (or relaxation) 2DES signal consists of both the rephasing and the nonrephasing components which are experimentally separated by the relative time ordering of pulses one and two. The rephasing portion is properly time-ordered signal where pulse one arrives before pulse two and the nonrephasing is collected when pulse two arrives before pulse one. Since pulses one and two have different k vectors, the signal produced in the $-k_1+k_2+k_3$ signal direction corresponds to a photon echo for the rephasing and a free induction decay for the non-rephasing signal. The total signal is a sum of both parts, producing a non-phase-twisted signal revealing the relaxation dynamics of the system.

The NV-diamond sample was synthesized (by Element Six) using a high pressure-high temperature method with an approximately 50 ppm nitrogen concentration. The sample was irradiated with 3 MeV electrons with a dose of 2x10^{19} cm^{-2} and annealed at 1325 K for two hours. This produced negatively charged NV-diamond centers with an optical density at room temperature of 0.06 at the zero-phonon line (638 nm, 15700 cm^{-1}) with an optical pathlength of 20 μm, as shown in Fig. 1(b). The optical density was determined from the linear absorption of the NV-diamond sample measured using a Varian Cary 50 UV-Vis Spectrophotometer. The 2DES experiments were performed using 60 nm or 1600 cm^{-1} full width half maximum spectral bandwidth pulses with a central wavelength of 625 nm or 16000 cm^{-1} and compressed to near transform limited sub 20 fs pulses at the sample position. The pulse was characterized using a frequency resolved optical gating (FROG) technique on a fused silica plate. The data was minimally processed and no interpolation or smoothing was applied to the 2D plots. 2DES measurements on a model dye system, oxazine 720 in methanol, were performed before and after the experiments on the NV-diamond sample to ensure experimental consistency. The t_1 time delay was scanned over $\pm$120 fs and 2DES surfaces were collected for t_2 time delays from 0 fs to 310 fs in 10 fs steps, from 325 fs

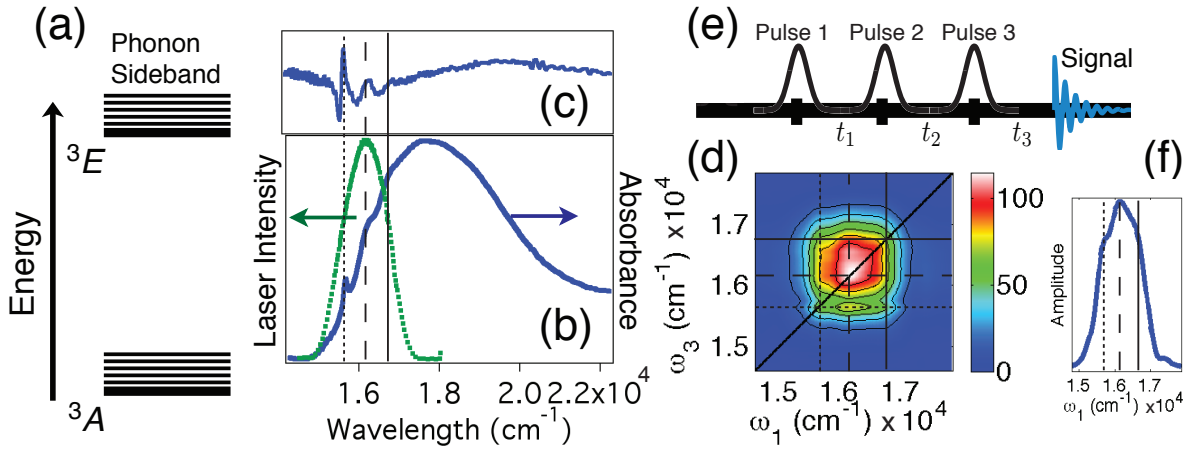

FIG. 1: Properties of the negatively charged NV center in diamond. (a) The level structure of the negatively charged NV defect in diamond including the vibrationally broadened spin triplet ^3E excited state and the ^3A ground state. The lowest energy, zero-phonon transition between the ground and the excited state produces a zero-phonon line in the absorption spectrum that persists to room temperature. (b) Room temperature absorption spectrum of the NV-diamond sample and the laser spectrum centered at 16000 cm^{-1} (625 nm) used in 2DES data collection. (c) Second derivative of the absorption spectrum, emphasizing the vibronic structure of the phonon sideband. (d) An absolute value 2DES plot of NV-diamond with a waiting time (t_2) of 5 ps. The intensity scale is in arbitrary units. The 2DES signal in (d) is plotted with respect to the detection axis, ω_3 and the absorption axis, ω_1. (e) The sequence of three pulses used to generate the third-order heterodyne nonlinear signal. (f) A slice through the 2DES plot in (d) along ω_1 at ω_3= 15700 cm^{-1} or the energy of the ZPL transition. The dotted, dashed and solid lines on panels (b), (c), (d) and (f) indicate the ZPL, the first and the second vibronic peaks as respectively as observed in the linear absorption.

to 400 fs in 25 fs steps, from 400 fs to 1.5 ps in 100 fs steps, at 1.8 ps, from 2 ps to 5 ps in 500 fs steps, from 5 ps to 10 ps in 1 ps steps, from 10 ps to 50 ps in 5 ps steps and from 50 ps to 100 ps in 10 ps steps. Each t_2 time was repeated a minimum of three times and the entire experiment was independently repeated five times. All experiments were performed at room temperature.

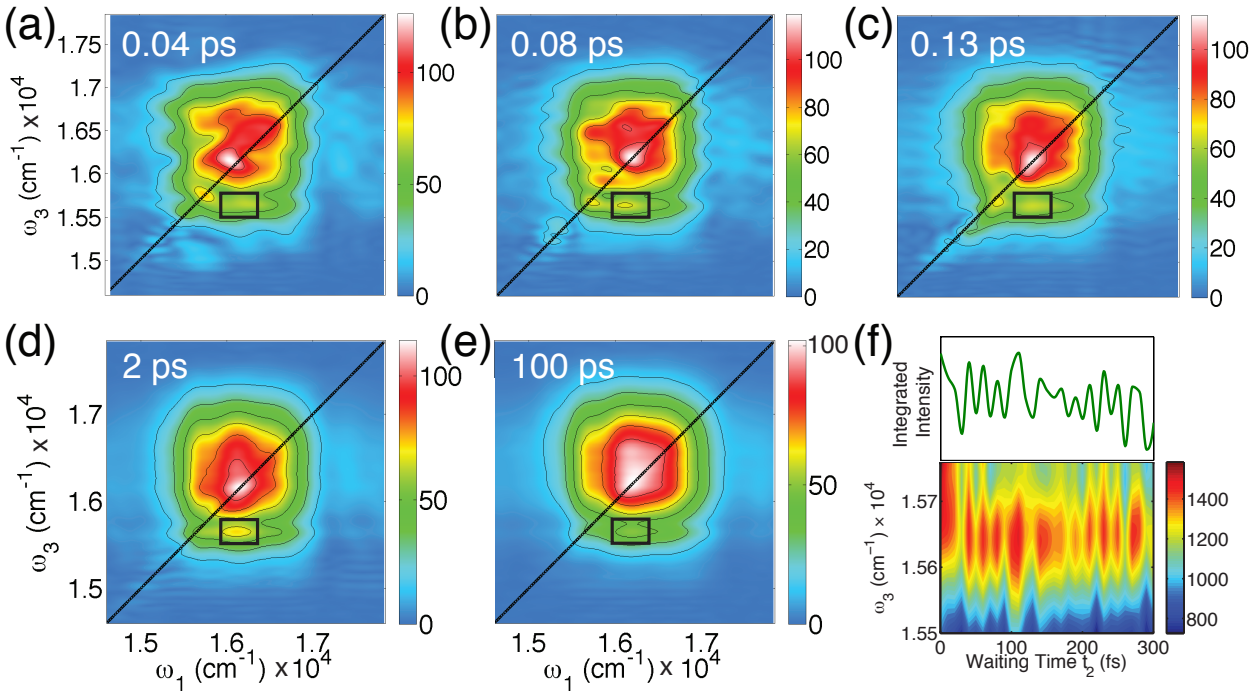

FIG. 2: 2DES measurement of NV defect centers. Panels (a) – (e) present representative absolute value total 2DES surfaces of NV-diamond at different waiting times, t_2, indicated in white. The intensity scale is in arbitrary units that are self-consistent within a set of experiments. At short waiting times ($t_2 < 2$ ps), the action of the vibrational modes is evident in the oscillating amplitudes across absorption and emission axes as the energy is redistributed amongst the vibrational degrees of freedom. After approximately 2 ps, the coherent vibrational dynamics driving the amplitude oscillations have relaxed and the 2DES signal assumes an asymptotic form dominated by the excited state population decay. The black boxes in panels (a) – (e) highlight the position of a vibronic cross peak, whose intensity oscillates with respect to the waiting time. Panel (f) shows the short waiting time oscillatory behavior of the boxed region obtained from the 2DES surfaces. The bottom part of (f) presents the signal obtained by integrating the boxed region over the ω_1 axis and plotting it relative to the ω_3 emission axis, while the top part shows the total integrated intensity of the same region.

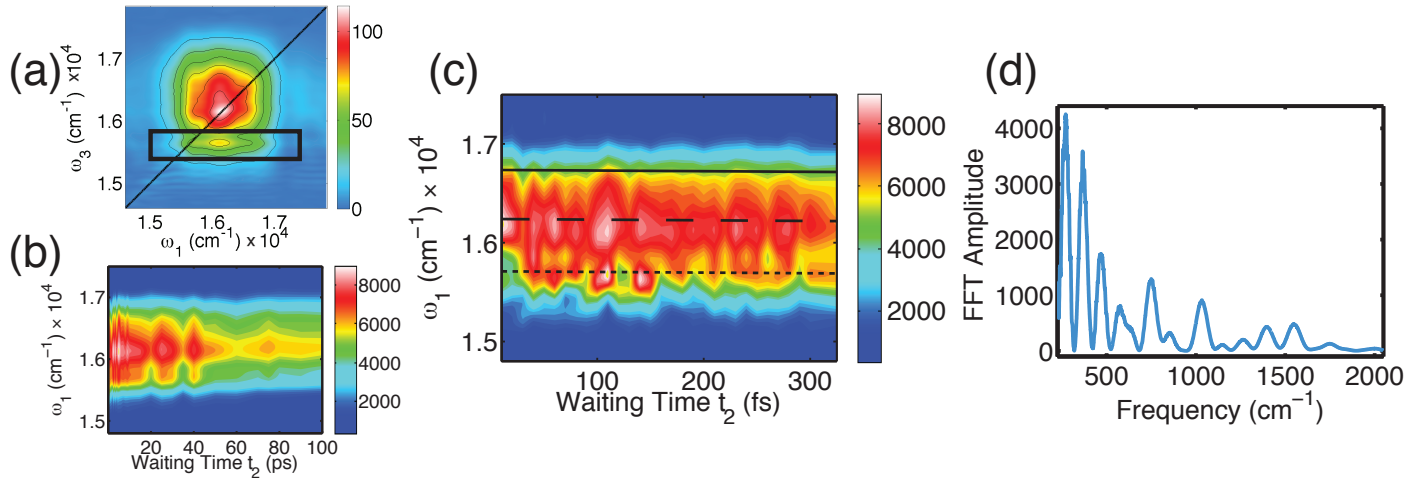

FIG. 3: Vibrational modes associated with emission at the ZPL transition energy. (a) The 2DES signal at t_2 =2 ps with a black box indicating the ZPL emission region. By integrating over the ω_3 axis for the ZPL emission region, vibrational dynamics associated with the ZPL transition energy can be isolated from the 2D signal. Panels (b) and (c) show representative plots of the integrated regions as a function of the waiting time, t_2. (b) The oscillations in the ZPL region to 100 ps with low frequency oscillations out to tens of picoseconds. (c) Shows the short time t_2 region of the same data presented in panel (b) displaying rich oscillations. The black lines indicate the diagonal peak, first and second vibronic cross peaks emitting at the ZPL transition frequency. Note that the pattern of black lines is the same as used in Fig. 1. Panel (d) shows the Fourier transform of the data in (c) integrated over the ω_1 axis.

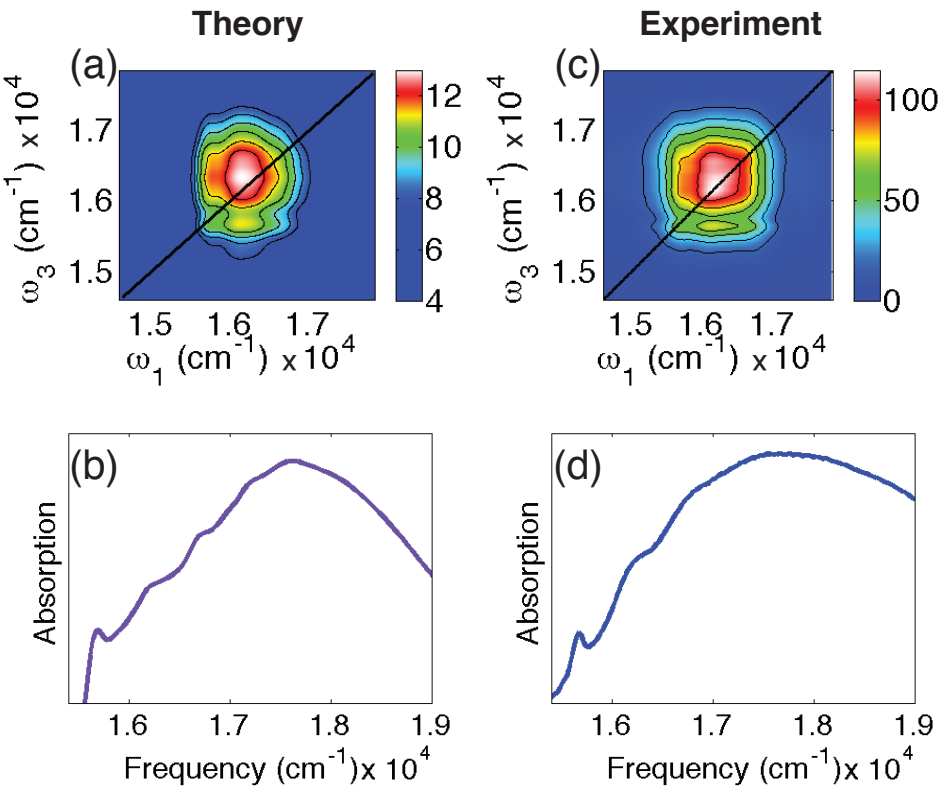

FIG. 4: Comparison between calculated and measured 2DES and linear absorption signals. Panels (a) and (b) show 2DES at t_2 =5 ps and linear absorption signals, respectively, calculated using discrete modes at frequencies recovered from the 2DES experimental data (see Fig. 3(d)). Panels (c) and (d) show the experimental 2DES measured at t_2 =5 ps and linear absorption signals, respectively.

* Current Address: Department of Chemistry and Biochemistry, University of Arizona, Tucson, AZ, USA 85721

† grfleming@lbl.gov

[1] Maurer, P. C. *et al.* Room-Temperature Quantum Bit Memory Exceeding One Second. *Science* **336**, 1283–1286 (2012).

[2] Fuchs, G. D., Dobrovitski, V. V., Toyli, D. M., Heremans, F. J. & Awschalom, D. D. Gigahertz Dynamics of a Strongly Driven Single Quantum Spin. *Science* **326**, 1520–1522 (2009).

[3] Childress, L. *et al.* Coherent Dynamics of Coupled Electron and Nuclear Spin Qubits in Diamond. *Science* **314**, 281–285 (2006).

[4] Gurudev Dutt, M. V. *et al.* Quantum Register Based on Individual Electronic and Nuclear Spin Qubits in Diamond. *Science* **316**, 1312–1316 (2007).

[5] Taylor, J. M. *et al.* High-Sensitivity Diamond Magnetometer with Nanoscale Resolution. *Nature Physics* **4**, 810–816 (2008).

[6] Balasubramanian, G. *et al.* Nanoscale Imaging Magnetometry with Diamond Spins under Ambient Conditions. *Nature* **455**, 648–651 (2008).

[7] Mizuochi, N. *et al.* Electrically Driven Single-Photon Source at Room Temperature in Diamond. *Nature Photonics* **6**, 299–303 (2012).

[8] Maurer, P. C. *et al.* Far-Field Optical Imaging and Manipulation of Individual Spins with Nanoscale Resolution. *Nature Physics* **6**, 912–918 (2010).

[9] Rand, S., Lenef, A. & Brown, S. Zeeman Coherence and Quantum Beats in Ultrafast Photon Echoes of NV Centers in Diamond. *Journal of Luminescence* **60&61**, 739–741 (1994).

[10] Lenef, A. *et al.* Electronic Structure of the NV Center in Diamond: Experiments. *Physical Review B* **53**, 13427–13440 (1996).

[11] Acosta, V. M., Jarmola, A., Bauch, E. & Budker, D. Optical Properties of the Nitrogen-Vacancy Singlet Levels in Diamond. *Physical Review B* **82**, 201202R (2010).

[12] Davies, G. & Hamer, M. F. Optical Studies of the 1.945 eV Vibronic Band in Diamond. *Proceedings of the Royal Society A: Mathematical, Physical and Engineering Sciences* **348**, 285–298 (1976).

[13] Collins, A. T., Stanley, M. & Woods, G. S. Nitrogen Isotope Effects in Synthetic Diamonds.

J. Phys. D: Appl. Phys. **20**, 969–974 (1987).

[14] Zaitsev, A. M. Vibronic Spectra of Impurity-Related Optical Centers in Diamond. *Phys. Rev. B* **61**, 12909–12922 (2000).

[15] Zhang, J., Wang, C.-Z., Zhu, Z. Z. & Dobrovitski, V. V. Vibrational Modes and Lattice Distortion of a Nitrogen-Vacancy Center in Diamond from First-Principles Calculations. *Physical Review B* **84**, 035211 (2011).

[16] Ginsberg, N. S., Cheng, Y.-C. & Fleming, G. R. Two-Dimensional Electronic Spectroscopy of Molecular Aggregates. *Accounts of Chemical Research* **42**, 1352–1363 (2009).

[17] Brixner, T., Mancal, T., Stiopkin, I. V. & Fleming, G. R. Phase-Stabilized Two-Dimensional Electronic Spectroscopy. *The Journal of Chemical Physics* **121**, 4221–4236 (2004).

[18] Cho, M., Brixner, T., Stiopkin, I. V., Vaswani, H. & Fleming, G. R. Two Dimensional Electronic Spectroscopy of Molecular Complexes. *Journal of the Chinese Chemical Society* **53**, 15–24 (2006).

[19] Rogers, L. J., Armstrong, S., Sellars, M. J. & Manson, N. B. Infrared Emission of the NV Centre in Diamond: Zeeman and Uniaxial Stress Studies. *New Journal of Physics* **10**, 103024 (2008).

[20] Kehayias, P. *et al.* Measurement of the ^1E to $^1A_1$ Phonon Sideband of the Nitrogen-Vacancy Center in Diamond. *submitted* (2012).

[21] Christensson, N. *et al.* High Frequency Vibrational Modulations in Two-Dimensional Electronic Spectra and Their Resemblance to Electronic Coherence Signatures. *Journal of Physical Chemistry B* **115**, 5383–5391 (2011).

[22] Farrow, D. A., Smith, E. R., Qian, W. & Jonas, D. M. The Polarization Anisotropy of Vibrational Quantum Beats in Resonant Pump-Probe Experiments: Diagrammatic Calculations for Square Symmetric Molecules. *The Journal of Chemical Physics* **129**, 174509 (2008).

[23] Bixon, M. & Jortner, J. Intramolecular Radiationless Transitions. *The Journal of Chemical Physics* **48**, 715 (1968).

[24] Gali, A., Simon, T. & Lowther, J. E. An Ab Initio Study of Local Vibration Modes of the Nitrogen-Vacancy Center in Diamond. *New Journal of Physics* **13**, 025016 (2011).

[25] Manson, N. B. & McMurtrie, R. L. Issues Concerning the Nitrogen-Vacancy Center in Diamond. *Journal of Luminescence* **127**, 98–103 (2007).

[26] Abtew, T. A. *et al.* Dynamic Jahn-Teller Effect in the NV-Center in Diamond. *Physical*

Review Letters **107**, 146403 (2011).

[27] Collins, A. T. & Woods, G. S. An Anomaly in the Infrared Absorption Spectrum of Synthetic Diamond. *Philosophical Magazine Part B* **46**, 77–83 (1982).

[28] Zaitsev, A. M. *Optical Properties of Diamond, A Data Handbook* (Springer, Berlin, 2001).

[29] Huxter, V. M. & Scholes, G. D. Acoustic Phonon Strain Induced Mixing of the Fine Structure Levels in Colloidal CdSe Quantum Dots Observed by a Polarization Grating Technique. *Journal of Chemical Physics* **132**, 104506 (2010).

[30] Jiang, X., Harzer, J. V., Hillebrands, B., Wild, C. & Koidl, P. Brillouin Light Scattering on Chemical-Vapor-Deposited Polycrystalline Diamond: Evaluation of the Elastic Moduli. *Applied Physics Letters* **59**, 1055–1057 (1991).

[31] Cho, M. *Two-Dimensional Optical Spectroscopy* (CRC Press, New York, 2009).

[32] Mukamel, S. *Principles of Nonlinear Optical Spectroscopy* (Oxford University Press, New York, 1995).

[33] Zhao, Y. & Knox, R. S. A Brownian Oscillator Approach to the Kennard-Stepanov Relation. *Journal of Physical Chemistry A* **104**, 7751–7761 (2000).

[34] Ye, J., Zhao, Y., Ng, N. & Cao, J. Width of Phonon Sidebands in the Brownian Oscillator Model. *Journal of Physical Chemistry B* **113**, 5897–5904 (2009).

[35] Jang, S., Cao, J. & Silbey, R. J. On the Temperature Dependence of Molecular Line Shapes Due to Linearly Coupled Phonon Bands. *Journal of Physical Chemistry B* **106**, 8313–8317 (2002).

[36] Brixner, T., Stiopkin, I. & Fleming, G. R. Tunable Two-Dimensional Femtosecond Spectroscopy. *Optics Letters* **29**, 884–886 (2004).

[37] Xu, Q.-H., Ma, Y.-Z. & Fleming, G. R. Heterodyne Detected Transient Grating Spectroscopy in Resonant and Non-Resonant Systems Using a Simplified Diffractive Optics Method. *Chemical Physics Letters* **338**, 254–262 (2001).